Characterization of coated soot particles

Validating a new APM software and using it to design aerosol measurement set-ups

Jakob Petersson

2015-2016

LUNDS UNIVERSITET

Jakob Petersson

MVEM45 Diploma work for Master degree 45 ECTS, Lund University

Intern handledare: Joakim Pagels, Ergonomics and Aerosol Technology, Lund University

CEC – Centre for Environmental and Climate Research
Lunds University
Lund 2015-2016

Abstract

Soot characteristics such as absorbing light are heavily dependent on its structure and interaction with other compounds. By coating soot or collapsing the soot core, the characteristics will be altered which affects its climate forcing, the lung deposition and other interactions with the human upper airways. In this work a new approach to measure aerosol particle mass with the Aerosol Particle Mass analyser (APM) was analysed and validated. A set-up was designed to coat soot particles with well-defined coating levels under controlled conditions. The new approach was used to prove restructuring of the soot core when coated by a hygroscopic compound and exposed to high relative humidity. Experiments were made with a Potential Aerosol Mass (PAM) chamber to simulate atmospheric aging of soot with the precursor alpha-pinene showing promising results of the combination PAM-APM.

Black carbon (BC) being the second most important climate forcer makes it crucial to map out its atmospheric interactions for future climate research. By applying coating to soot the absorption rate of light can increase with 100% since the coating works as a lens focusing the light into the black soot core. Black carbon being associated with $PM_{2.5}$ is linked to decreased lung function, increased respiratory symptoms and cardiopulmonary diseases.

Table of Contents

Contents

List of Abbreviations

APM – Aerosol Particle Mass analyser

BC – Black Carbon

CO_2 – Carbon Dioxide

CPC – Condensation Particle Counter

CPMA – Couette centrifugal Particle Mass Analyser

DMA – Differential Mobility Analyser

DOS – Dioctyl Sebacate

Lpm – Liters per minute

OP – Operation Point

PAM – Potential Aerosol Mass

PSL – Polystyrene Latex spheres

RH – Relative Humidity

RPM – Rounds Per Minute

SA – Succinic Acid

SMPS – Scanning Mobility Particle Sizer

SOA – Secondary Organic Aerosol

VOC – Volatile Organic Compound

Introduction

Soot particles are widely studied for their impact on Earth's radiation balance and health aspects. When fresh soot is released to the atmosphere it will react with ambient substances which change the property of the soot particle (Mikhailov et al., 2006; Zhang et al., 2007; Fan et al., 2008). Soot is introduced to the atmosphere through various combustion processes such as engines fueled by diesel (Kittelson, 1998) or spark ignition engines (Kittelson et al., 2006), biomass combustion (Wierzbicka et al., 2005), and indoor combustion for example candle burning (Pagels et al., 2009). Soot particles can also be generated under controlled conditions using laboratory scale burners (Maricq et al., 2003).

In this study, soot is generated by a miniCAST Model 5201 Type C (Jing, 2006). The soot is then analysed using an Aerosol Particle Mass Analyser (APM) in terms of characteristics such as relationships between mass, effective density and mobility diameter (Ehara et al., 1996; McMurry et al., 2002). The APM was introduced by Ehara et al. (1996) and consists of two concentric rotating cylinders with the same rotation speed. A voltage is applied to the inner cylinder which is used to balance the centrifugal force in order to measure mass of aerosol particles passing through the APM.

The original APM software allowed the user to scan aerosol particle masses by changing the voltage applied to the inner cylinder. A new software was recently developed at Lund University and offers the user to scan either the mass or effective density changing the rotational speed of the system. The new software is not yet experimentally tested and needs to be validated before new tests are run. The software development is inspired by the article written by Kuwata (2015) indicating the benefits of varying the rotational speed rather than the voltage of the APM.

It is suggested by Bond et al. (2006) on theoretical grounds that soot coated by other particles can absorb about 100% more light than fresh soot particles leading to an enhancement of the radiative forcing however this relationship requires detailed experimental verification. It is further proposed by Bond et al. (2013) that the short-lived climate forcer BC, which is the main component in soot, is the second most important climate forcer from human emission with the most important being carbon dioxide (CO_2). In contrast to CO_2 having a life time of decades, BC is a short-lived climate forcer due to the short life time of up to a few weeks of aerosol particles in the atmosphere.

This study is important for the increased knowledge of aerosol characteristics and potential applications for further research. Humans together with other animals and man-made products are exposed to aerosols constantly which intensify the need of being able to fully comprehend what effects different aerosols leads to. Soot particles are emitted globally through various forms of combustion and can react with substances. By adding different coatings to the soot particles, this study will try to map out the changes of the aerosol particle properties.

Purpose

The purpose with this study is to:

- Validate the method of scanning aerosol particle masses and densities by changing the APM rotation speed instead of the voltage.
- Characterise fresh soot with different properties
- Characterise soot coated by single compounds
- Characterise soot coated by atmospheric-like Secondary Organic Aerosol (SOA) mixture

Background

In order to properly analyse soot, the equations associated with the soot structure is revised in this chapter. The general equations for aerosol particle behaviour are collected from Hinds (1999) and the applied equations for soot particles from various journal articles.

Soot characteristics

Soot is an agglomerate of roughly spherical primary particles (Park et al., 2004b) which are bound by Van der Waals forces (Totton et al., 2009). The size of the primary particles is typically 5-60 nm (Barone et al., 2007) depending on the conditions of the combustion such as fuel-to-air ratio (Schnitzler et al., 2014). Soot will experience more coating processes the longer it is residing in the atmosphere by condensation or deposition from other airborne gases or aerosols. Coating will change the morphology of the soot together with the chemical and optical properties such as the proficiency of forming clouds or the ability to scatter light (Cross et al., 2010). The density of soot was measured to be 1.77 g/cm^3 by Park et al. (2004b).

Aerosol properties

The mass of a non-spherical aerosol can be calculated by the relationship of effective density, ρ_{eff}, electric mobility diameter, d_{me}, and the particle mass, m_p (McMurry et al., 2002):

$$m_p = \frac{1}{6}\pi\rho_{eff}d_{me}^3 \quad (1)$$

The electric mobility is a measure of mobility that depends on size and shape factor (Pagels et al, 2009) described later in equation 9. The relationship between mass and effective density is linear but the electric mobility diameter is to the power of three, thus any minor error in obtaining the diameter will greatly affect the mass or density values (McMurry et al., 2002).

Equation 1 can be rewritten on a logarithmic scale to give a linear relationship (Kuwata, 2015):

$$\log m_p = \log \frac{1}{6}\pi + \log \rho_{eff} + 3 \log d_{me} \quad (2)$$

The linear relationship is used to define the mass-mobility exponent D_m given by a modification of equation 2 (Park et al 2004a, Kuwata, 2015):

$$m_p = \rho_f d_{me}^{D_m} \leftrightarrow \log m_p = \log \rho_f + D_m \log d_{me} \quad (3)$$

The D_m equals 3 for a spherical particle and a smaller value for a non-spherical particle, generally in the range of 2.2-2.4 for fresh soot (Park et al., 2003). The ρ_f term is a pre-exponential factor that equals $1/6\,\pi\rho_{eff}$ when D_m = 3 rendering equation 3 a generalized form of equation 2 (Kuwata, 2015).

Stoke's Law

Stokes's law describes a state where the inertial forces are negligible compared with the viscous forces for a spherical particle. The ratio between inertial forces and viscous forces is known as the Reynolds number and achieving negligible inertial forces is implied by a low Reynolds number. The law is derived from the Navier-Stokes equation and can be solved linearly thanks to the negligible inertial forces. The law can be described by equation 4 (Hinds, 1999):

$$F_D = 3\pi\eta V d \quad (4)$$

where F_D is the drag force, η is the viscosity for the medium; V is the velocity and d the diameter of the aerosol particle.

Stokes's law assumes that the relative velocity of the gas at the surface of the particle is zero, this is not true for small particles whose size approaches the mean free path of the gas because there is a "slip" on the surface and this needs to be corrected for (Hinds, 1999). This is done by the Cunningham slip correction factor C_c (Allen & Raabe, 1982, 1985):

$$C_c = 1 + Kn\left[1.165 + 0.483exp\left(-\frac{0.997}{Kn}\right)\right] \quad (5)$$

It is stated that the slip correction factor should be used for particles smaller than 5-10μm, for a 1.0μm particle the C_c factor is 1.15 at standard conditions and increases as the size of the particle decreases (Hinds 1999). The slip correction factor is coupled with the Knudsen number that describes the flow regime of the gas around the particle. The dimensionless Knudsen number is a ratio between the mean free path of gas, λ, and the particle size, d (Allen & Raabe, 1985; DeCarlo, 2004):

$$Kn = \frac{\lambda}{d} \quad (6)$$

The mean free path is the average distance travelled by the particle between successive collisions and is calculated from (Hinds, 1999):

$$\lambda = \frac{1}{\sqrt{2} n_v \pi d_m^2} \quad (7)$$

For a given gas, meaning a fixed collision diameter d_m, λ depends only on the gas density which is proportional to the number of molecules per unit volume, n_v (Hinds 1999).

The flow regimes around the particle can be divided to three regimes depending on the Knudsen number, *Kn* (DeCarlo, 2004):

$Kn \ll 1$	$0.1 < Kn < 10$	$Kn \gg 1$
Continuum regime	Transition regime	Free-molecular regime

In the continuum regime, the Knudsen number is small leading the correction slip factor being close to 1 meaning that the collisions between the particle and the gas are discrete. In the transition regime and the free-molecular regime the Knudsen number will be significant and the Cunningham correction slip factor will be larger than 1 and will affect the drag force by (DeCarlo, 2004):

$$F_D = \frac{3\pi\eta V d}{C_c} \quad (8)$$

The experiments in this study take place in the transition regime emphasising the effects of the Cunningham correction slip factor.

Dynamic shape factor

Soot is not a spherical particle so Stokes's law requires further modification. The dynamic shape factor, χ, is the ratio of the actual drag force for a non-spherical particle and the drag force for a sphere with the same volume and velocity as the non-spherical particle. The dynamic shape factor can be expressed as (DeCarlo, 2004; Pagels et al., 2009):

$$\chi = \frac{d_{me}}{d_{ve}} \cdot \frac{C_c(d_{ve})}{C_c(d_{me})} \quad (9)$$

where d_{ve} is the equivalent volume diameter which is defined as the diameter of a sphere having the same volume as a non-spherical particle (Hinds, 1999). For spherical particles $\chi = 1$ and $d_{me} = d_{ve}$ and for non-spherical particles $\chi > 1$ and $d_{me} > d_{ve}$ (McMurry et al., 2002).

Condensation

The most important transfer of gases to particles is condensation. The process requires a supersaturated vapour in the presence of particles which will act as condensation surfaces (Hinds, 1999). The condensation is governed by the saturation vapour pressure, also called vapour pressure, which is defined as the pressure needed to maintain a vapour in mass equilibrium at a specified temperature (Hinds, 1999).

When the partial pressure, the pressure a gas exerts in a mixture if that gas was the solemn occupant, equals the saturation vapour pressure there is mass equilibrium at the surface. In order for a vapour to be supersaturated the partial pressure needs to be greater than the vapour pressure. To obtain condensation in controlled experiments, a gas is cooled down which lowers the vapour pressure while the partial pressure is unaffected (Hinds, 1999).

The saturation vapour pressure is defined for a flat surface at a specified temperature. For a particle where the surface is curved, the partial pressure must be greater than the vapour pressure in order to obtain mass equilibrium which is known as the Kelvin effect (Hinds, 1999). It is suggested that the negative curvature of soot particles enhance the condensation of water and other chemical components onto its surface, primarily for larger particles (Zhang et al., 2008).

Homogeneous nucleation

Homogeneous nucleation is the process when particles form in a supersaturated vapor without ambient condensation nuclei. Molecular forces will lead to formations of unstable clusters which disintegrate unceasingly. When such cluster formations exceed a critical size it will become stable and grow by condensation (Hinds, 1999).

Instrumental theory

Differential Mobility Analyser

The Differential Mobility Analyser (DMA) is an instrument that filtrates out particles with a specific mobility diameter d_{me} by classifying the electrical mobility, Z, through the relationship between size and voltage. The electrical mobility is defined as (Knutson & Whitby, 1975):

$$Z = \frac{neC_c}{3\pi\mu d_{me}} \quad (10)$$

where n is the number of elementary charges, e is the unit electric charge and μ the absolute viscosity of air. To obtain the electrical mobility the relationship with voltage is used:

$$Z = \frac{Q_{sh,DMA}\ln(r_{2\_DMA}/r_{1\_DMA})}{2\pi V_{DMA}L_{DMA}} \quad (11)$$

where Q_{sh} is the sheath flow of air running through the DMA, r_1 and r_2 the radii of the electrodes, V the voltage applied over the DMA and L the length of the cylinders.

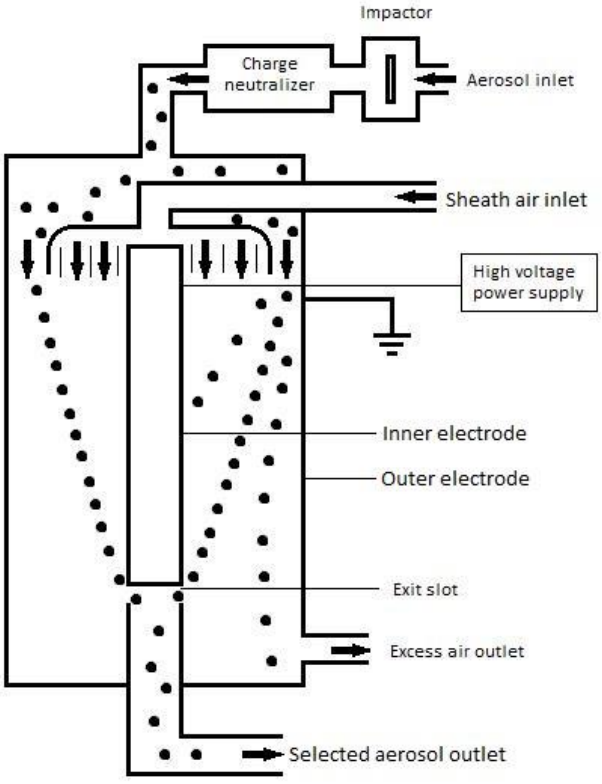

Figure 1 DMA schematics

The aerosol particles are marked as dots and the pathway illustrated by arrows. The sheath air, or clean air, is mixed with the aerosols in the classifier section and will remove unwanted aerosols by the excess air slot.

Aerosols particles are introduced to the electrostatic classifier described in Figure 1 through an inlet and passes through an impactor where too large particles are

removed. The remaining aerosols are neutralized to the Boltzmann equilibrium charge distribution by a charge neutralizer so that most particles are singly charged (McMurry et al., 2002), they are then sent through the electrostatic classifier section together with a flow of sheath air. A high voltage supply will create an electric force pulling the aerosols with different magnitudes depending on the particle mobility diameter (Hinds, 1999).

Aerosols particles with the desired mobility diameter corresponding to the set up voltage will be able to pass through an exit slot and leave the DMA while aerosols with too small and too large diameters will hit mechanical obstacles in the DMA and leave through an outlet. The aerosol particles that pass through the DMA will be of a known size distribution and mostly singly charged (Hinds, 1999).

The DMA:s used in this work was the TSI Electrostatic Classifier 3071 (TSI Ltd.)

Aerosol Particle Mass analyser

After the DMA, the size selected particles enter the APM (Figure 2) through an inlet between the cylinders with the same rotation speed and will experience two opposite directed forces. In order for particles to penetrate through the APM, the inward generated electrostatic force must equal the outward driven centrifugal force for particles of a given mass. This is done by varying either the voltage given the inner cylinder or the rotational speed of the system, this will occur at the equilibrium radius (Ehara et al., 1996).

The equilibrium radius is defined as the particular radius from the center of the APM where the centrifugal force equals the electrostatic force. For a fixed setting of voltage or rotational speed, particles with a specific mass enters the APM at the equilibrium radius and will pass through unaffected since the opposite forces cancels out (Olfert & Collings, 2005). Particles with a lower mass will experience a weaker centrifugal force and will hit the inner cylinder and particles with a larger mass will collide with the outer cylinder since the centrifugal force is stronger than the electrostatic and neither will pass through.

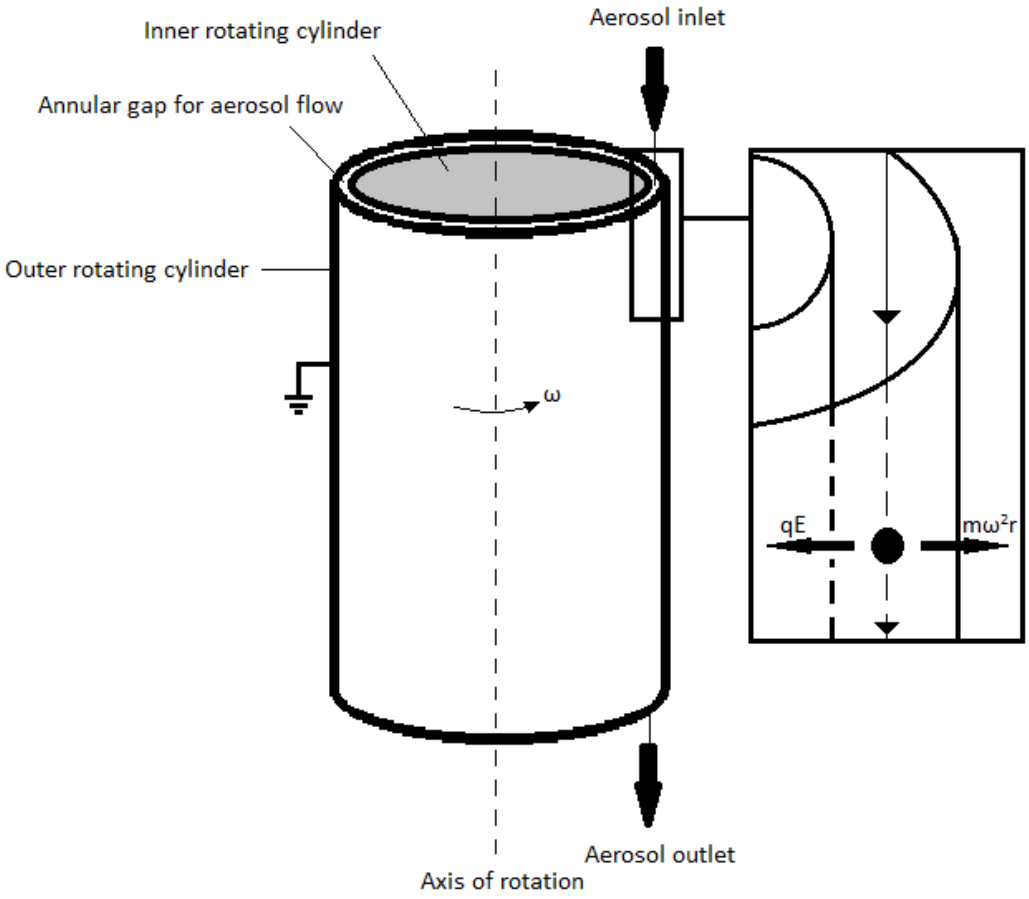

Figure 2 APM schematics

The aerosol illustrated as a dot in the zoom up is experiencing two equally strong forces balancing it on the equilibrium radius.

A study by Kuwata (2015) urges that by keeping the classification performance parameter λ_c derived by Tajima et al. (2012) constant, the resolution and shape of the APM transfer function formulated by Ehara et al. (1996) will be constant while scanning. The APM transfer function describes the probability of a particle with certain mass and charge to pass through the APM without depositing on the rotating electrodes with respect to the geometry and operating conditions of the APM. The APM classification is governed by both V_{APM} and ω which implies that m can be determined by keeping one constant and the other as a variable. Kuwata (2015) showed that λ_c stay constant when V_{APM} is constant and ω is a variable to determine m.

For the APM model 3600 (Kanomax Ltd.) the APM rotation speed is limited to the interval 50-9500 rounds per minute (RPM) in order to keep the motor under stable conditions. The voltage range is between 0.3 V and 2 kV, the upper limit is to make sure there will be no electrical discharge between the cylinders and the

lower is determined by the resolution of the voltage control by a computer (Tajima et al., 2011).

Dilution system

The DMA:s are prone to clogging if the number of particles running through is too high. The Dekati Diluter DI-1000 (Dekati Ltd.) uses low pressure caused by a pressurised dilution air flow to draw in the sample and dilute it as seen in Figure 3. Diluted samples will exit the diluter pulled by the flow controlled by the system and the rest will leave by an exhaust outlet (Dekati, 2016a).

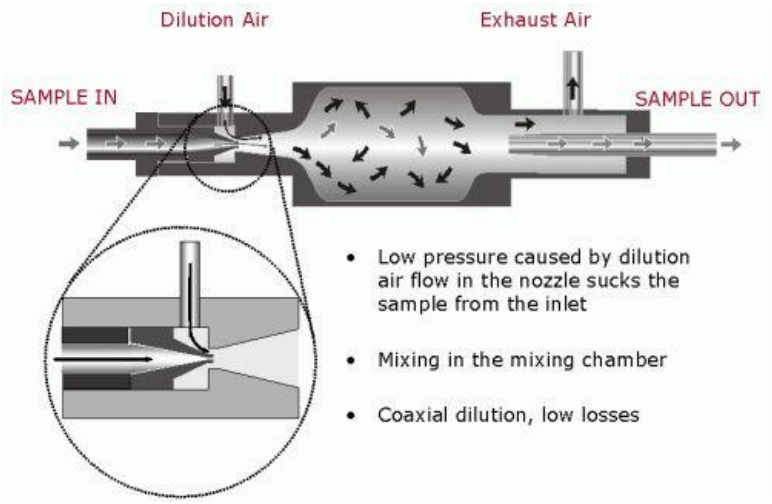

Figure 3 Schematics of the Dekati Diluter DI-1000
The aerosol pathway is marked by arrows, where the black arrows represent particles leaving the system through the exhaust outlet and grey arrows representing sample particles remaining in the system to be measured by the set-up (Dekati, 2016b).

Impinger

The impinger is glassware containing either water or an organic solvent used to expose an introduced aerosol particle to high saturation of the contained substance. The aerosol flow is directed through a nozzle on the impinger, bubbling it through the substance within as shown in Figure 4. The aerosols are then exposed to saturated vapours above the substance level before exiting the impinger (Miljevic et al., 2011).

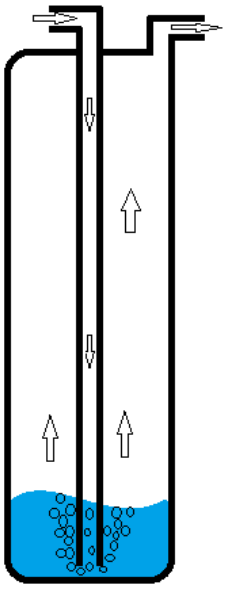

Figure 4 Impinger

The aerosol pathway is marked by arrows, starting through an inlet of a small glass pipe leading to the bottom of the glassware where it is introduced to the substance. The aerosol will bubble to the surface and then exit through the outlet.

Potential Aerosol Mass Chamber

PAM is a concept introduced by Kang et al. (2007) studying the formation of secondary aerosol mass. In the PAM oxidation flow reactor a Volatile Organic Compound (VOC) is introduced where atmospheric ageing is simulated by controlling UV-lamps and relative humidity (RH), but with the timescale reduced from days or hours down to a few minutes (Kang et al., 2007). O_3 is produced internally by a UV-lamp set on the wavelength 185nm in the chamber where further photolysis of the ozone forms excited oxygen radicals ($O(^1D)$) by a UV-lamp set on wavelength 254nm (Lambe et al., 2010). The $O(^1D)$ radicals will react with water vapour from the high RH producing OH radicals. The inserted VOC will oxidize with both O_3 and OH to form SOA within the PAM chamber (Lambe et al., 2010).

In this thesis the PAM chamber was investigated for its suitability for coating soot particles with SOA formed from oxidation of alpha-pinene.

Method and Experimental Set-up

Initial calculations made by equation 1 and 4-11 will lay the foundation of the calibration and instrumental boundaries used for the experimental set-ups.

PSL Calibration

In order to calibrate the system, a particle of known characteristics must be analysed by the instruments. The Polystyrene Latex spheres (PSL) serves this purpose as the particles are spherical with the density 1.054g/cm^3 (McMurry et al., 2002).

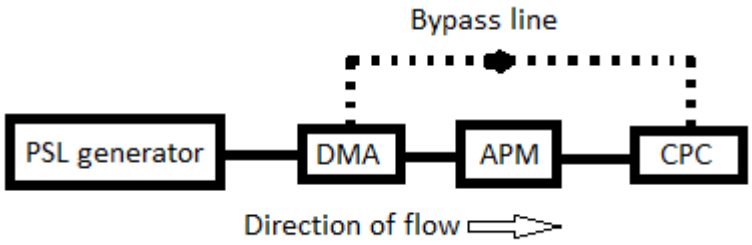

Figure 5 Set-up for PSL calibration.
The aerosol particles are generated in the PSL generator and are then dried and transported in the direction of the flow. The bypass line (dashed) is used when performing a DMA-CPC scan.

The PSL set-up as seen in Figure 5 is run by the flow control of the Condensation Particle Counter-pump (CPC) and pressurised air connected to the nebulizer. The aerosol flow is set to 1.0 liters per minute (lpm) by the CPC pump. The PSL particles are suspended in a surfactant solution which is diluted by distilled water and then run through a combination of a nebulizer and a dryer acting as a PSL generator making the particles airborne as an aerosol ready to enter the DMA.

The DMA voltage is set in the APM software and the APM is run for both the volt vector and the RPM vector for each PSL size measuring the mass of the

particles. The measured mass is compared to the theoretical mass of PSL particles derived using equation 1.

McMurry et al. (2002) designed an approach to obtain the effective density of a particle of interest, $\rho_{aerosol}$, from a relationship with the known PSL mass (m_{PSL}) and density (ρ_{PSL}) and the measured aerosol particle mass $m_{aerosol}$:

$$\rho_{aerosol} = \rho_{PSL}\frac{V_{aerosol}}{V_{PSL}} \leftrightarrow \rho_{aerosol} = \rho_{PSL}\frac{m_{aerosol}}{m_{PSL}} \quad (12)$$

The left hand side is the original approach by McMurry et al. (2002). It had to be modified in this experiment when scanning RPM by using the obtained mass rather than voltage ($V_{aerosol}$ and V_{PSL}), both sides are equivalent since the mass is proportional to the voltage. For each APM mass distribution, a peak value was obtained from a MATLAB fitted curve which was then used in equation 12 to determine the effective density.

Analysis of fresh soot

The soot generator, miniCAST (Jing Ltd.), was installed and run through the DMA-APM-CPC to obtain a mass spectrum for soot with different mobility diameters. The soot generator can run seven different Operation Point (OP) modes to form different soot particles by changing the mixing flow rates of propane, nitrogen and air (Jing, 2006). OP mode 1, 3 and 6 (Table 1) were analysed by the APM for different sizes where OP 1 is the most diesel-like, similar to the soot measured by Park et al. (2004b). The combustion temperature decreases with the increasing OP number having a higher flow of the cooling gases nitrogen and mixing air affecting the characteristics of the soot (Moore et al., 2014).

Table 1 miniCAST OP mode flow levels

The flow of fuel for each OP mode. The flows are acquired from the instructions manual for the miniCAST Model 5201 Type C by JING.

Fuel flow	OP 1	OP 3	OP 6
Propane (lpm)	0.06	0.06	0.06
Nitrogen (lpm)	0	0.1	0.25
Mixing air (lpm)	1.55	1.52	1.42

A Scanning Mobility Particle Sizer (SMPS) system was set parallel to the DMA-APM-CPC system to observe the stability of the system. The SMPS consists of a

DMA and a CPC which will analyse the size distribution of the aerosols as can be seen in Figure 6. The pump in the SMPS CPC is set to 0.3 lpm and together with the CPC-pump on the APM line the net aerosol flow of the system equals 1.3 lpm. A dilution system is connected to prevent clogging the DMA:s with soot and reducing the amount of remaining traces from previous runs since this may cause uncertainties in the next measurements. A cyclone separator was used in combination with the ejector diluters to prevent the ejector diluter nozzles from clogging.

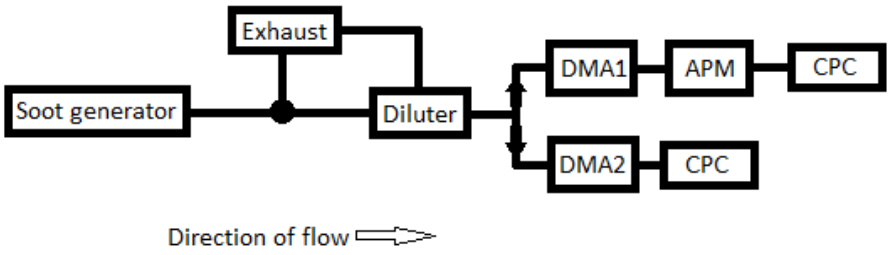

Figure 6 Fresh soot set-up

An exhaust point is removing the excess aerosols from the system, it is connected both to the tube between the soot generator and on each ejector diluter in the dilution system. It does not affect the aerosol flow generated by the CPC pumps. After the dilution system the flow is split up into two parallel lines where the two CPC pumps decide the ratio of aerosols transported each way.

After the measurement, the effective density is calculated from the particle mass obtained by the APM, first for the PSL and then for the soot of the same mobility size, given by the relation from the PSL calibration.

Initial coating stage with single compound

In order to analyse soot coatings a new set-up had to be designed. The focus of the design was to coat the soot on a small scale requiring only small volumes coating material in order to keep costs of substances down without affecting the quality of the experiment.

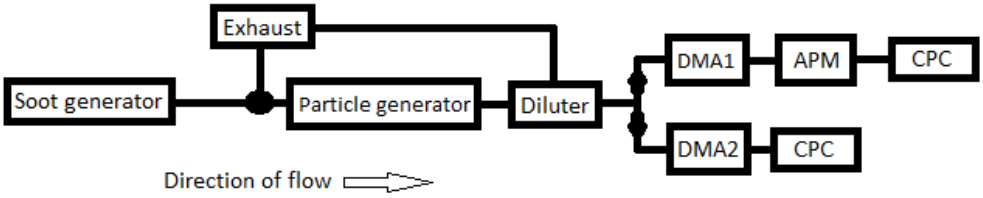

Figure 7 Initial coating set-up

The only modification from Figure 6 is the Particle generator between the exhaust point and the dilution system.

A patent pending particle generator is introduced to the set-up as seen in Figure 7. The generator consisted of a metal chamber where a substance of interest is put. The metal chamber is heated up to a wanted temperature by resistively heating in order to evaporate the substance. Soot is run through the metal chamber and the aerosol is cooled down by heat exchange with the surrounding metal pipes transporting the mix to the DMA. The particle analysed in the APM is referenced as the particle size chosen by DMA1. The aerosol flow remained at 1.3 lpm.

The substance chosen was Succinic Acid (SA) for the research value. It is a solid hygroscopic salt (Riipinen et al., 2006) with density 1.572 g/cm^3 (Pubchem., 2016) and low vapour pressure making it suitable for condensation purposes.

Improved coating stage with single compounds

After initial tests the set-up proved non-stable with the main issue being the particle generator not having the capacity for the amounts of soot being emitted. The particle generator dimensions were therefore modified to manage the high amount of soot passing through. The dilution system and the DMA from the APM line were put before the particle generator to reduce the concentration as shown in Figure 8 where initial tests yielded satisfactory amounts of soot. The new position of the DMA changed the size distribution of soot in the coating system to monodisperse.

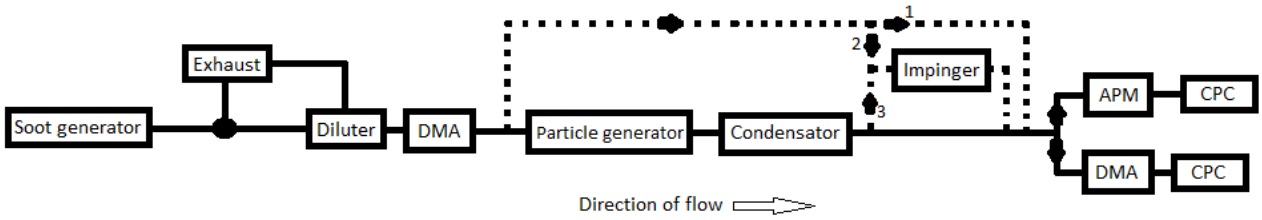

Figure 8 Improved coating set-up

The particle generator is repositioned as well as the DMA from the APM line compared to the initial coating stage in Figure 7. A series of bypass lines allows the user to run fresh soot bypass the particle generator and bypass (1) or through (2) the impinger. Another bypass line (3) allows the user to run coated soot through the impinger.

The cooling system was exchanged with the SLG 270 (TOPAS, 2016) where the particle generator parts were removed. The reason why the particle generator part from the SLG 270 was removed was that it is designed for larger quantities of liquids producing much larger particles (50-500nm) than the ones of interest in this experiment. The parts taken from the SLG were the reheater which heats up the aerosols to result in complete evaporation of the substance and a long glass tube offering effective passive cooling resulting in a well-defined condensation profile for the system. The total flow rate through the system was the combined flow of the CPC:s, set to 1.55 lpm for the SMPS CPC pump and 1.0 lpm for the APM CPC pump resulting in a total flow of 2.55 lpm.

Dioctyl Sebacate (DOS) together with Succinic Acid (SA) were chosen for their different characteristics, DOS being a hydrophobic liquid with the density 0.914 g/cm^3 (Pubchem., 2016) having a known coating profile (Ghazi & Olfert, 2013) to validate the system, SA a hygroscopic solid to challenge the soot structure. The influence of high RH on the soot morphology was analysed by running the coated soot and uncoated soot on a bypass line through an impinger (Miljevic et al., 2013).

The first coating experiments were related to the work of Ghazi & Olfert (2013) where fresh soot was coated by DOS oil. The mass of the soot particles was first measured with APM bypass the particle generator. Then the particle generator was heated up to different temperatures to yield different coating levels and the coated particle mass was measured with the APM. The purpose of the SMPS system is extended to observe size growth and not only stability of the system. After the coating scans the soot was run bypass the particle generator again to evaluate the stability of the system. The mass growth factor (*Gfm*) as seen in equation 13 is derived from the change in mass between the coated soot particles (m_{coated}) and the soot particles run bypass (m_{fresh}) the particle generator.

$$Gfm = \frac{m_{coated}}{m_{fresh}} \quad (13)$$

Coating with complex Secondary Organic Aerosol using PAM chamber

The set-up was redesigned to use a PAM chamber (Figure 9) to fill the function of the particle generator from the previous experiments. Soot was introduced into the chamber together with a quench flow of air and alpha-pinene (a precursor that will form Secondary Organic Aerosol in the chamber). The amount of alpha-pinene in the system was controlled by the total flow of quench air and alpha-pinene. DMA1 was repositioned to the APM line again resulting in a polydisperse size distribution of coated soot. A few tests were also made with the DMA1 put between the Dilution system and the junction where the gases were mixed to observe the option of running the system with monodisperse size distribution for coated soot.

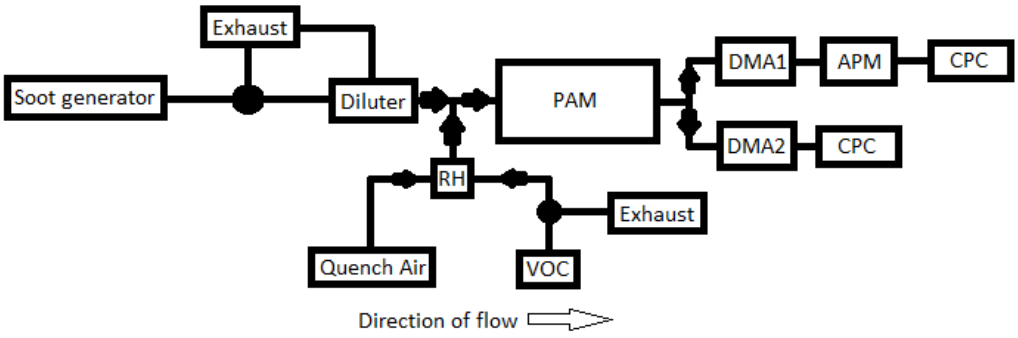

Figure 9 PAM coating set-up

Two exhaust points are removing unwanted levels of soot and alpha-pinene (VOC). The flow of aerosols is marked by arrows at the junctures.

Alpha-pinene was chosen for its known characteristics as being one of the most important precursors for SOA formation, primarily released from pine forests. Two vials were prepared with different dimensions to yield two levels of alpha-pinene to the system. The PAM had been calibrated to 5 lpm from previous PAM experiments which was achieved by the total flow of the pumps from both the CPS:s and a vacuum point at the PAM outlet. The soot flow was determined by the total flow deducted by the alpha-pinene flow and quench air flow.

The alpha-pinene levels could be set by two approaches, either by inserting new vials of alpha-pinene which was chosen for this experiment or by varying the flow of alpha-pinene. The approach of varying the flow introduced the human error since the flow was changed manually; therefore the multiple vial approach was chosen.

Results and Discussion

Before calibrating the system, calculations were made according to equations 1 and 4-11 which can be seen in appendix I to obtain reference values of arbitrary characteristics between: masses, mobility sizes and effective densities. The calculations resulted in different run vectors to be used in the APM software for both the old approach with varying the APM voltage and the new approach where the APM RPM is varied.

The DMA voltage output was examined by manually increasing the voltage while probing with a voltmeter (*Velleman DVM92 model IEC1010)*. The DMA was further examined by a DMA-CPC scan to measure which DMA voltage that let PSL particles of known sizes through and can be seen in Appendix II.

Different nozzle sizes were investigated for their dilution ratio and can be seen in Appendix III, nozzle 3 and 4 were used to keep the amount of soot particles on a satisfactory level.

The fitted curves presented in this section are purely for comparison, a MATLAB code provided fitted curves with peak values used for calculations.

APM measurement of PSL

The two approaches, voltage scan and RPM scan, for measuring the mass agreed well for every scan. The scans for 350nm PSL particles are shown in figure 10. The RPM setting resulted in a slightly broader distribution but very smooth. The reason for the voltage scan being narrower and less smooth may be because the varying resolution impacts the number of particles in the bins close to the peak bin.

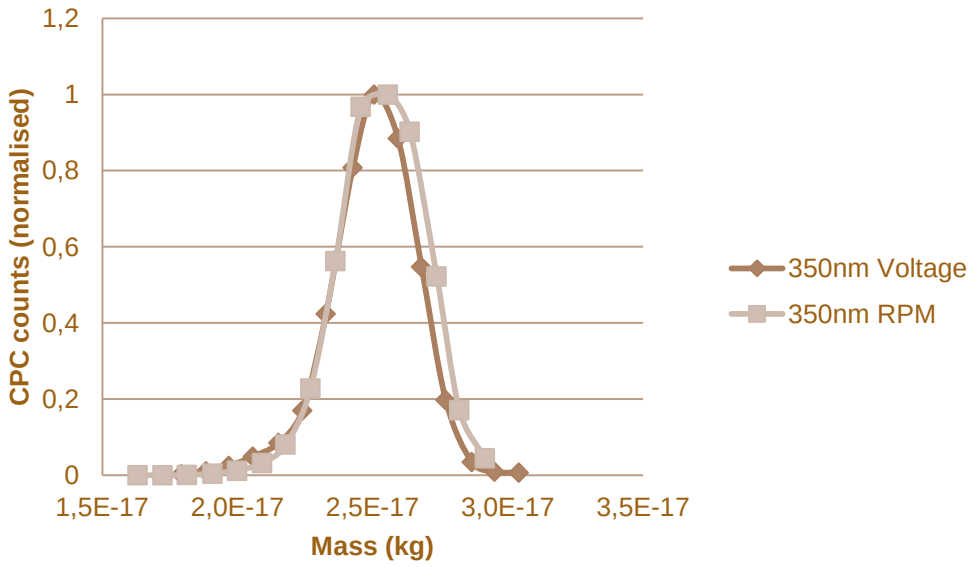

Figure 10 PSL mass distributions

The mass distribution for the 350nm PSL particles obtained from both scanning RPM and scanning voltage agreed well with only minor differences.

Both settings agreed well for every PSL size and all eight runs showed an overestimation of the theoretical mass for the PSL particles showed in table 2 of 7-15 % which could be a result of impurities on the PSL particle surfaces. The mass scans with the RPM setting falls within a margin of [1.5%] from the mass scans with the Voltage setting.

Table 2 PSL mass measurements

The calculated theoretical mass for all PSL sizes and the mass obtained for each size from both scanning RPM and scanning voltage. The two settings are compared in the last column by dividing the RPM scan with the Voltage scan for each size.

PSL size (nm)	Mass theoretical (kg)	Mass Voltage Scan (kg)	Mass RPM Scan (kg)	Mass offset Voltage Scan	Mass offset RPM Scan	Difference RPM/Voltage
80	$2.81 \cdot 10^{-19}$	$3.24 \cdot 10^{-19}$	$3.22 \cdot 10^{-19}$	15.2%	14.3%	-0.79%
100	$5.50 \cdot 10^{-19}$	$6.33 \cdot 10^{-19}$	$6.29 \cdot 10^{-19}$	15.1%	14.4%	-0.67%
240	$7.60 \cdot 10^{-18}$	$8.12 \cdot 10^{-18}$	$8.23 \cdot 10^{-18}$	6.90%	8.33%	1.33%
350	$2.36 \cdot 10^{-17}$	$2.52 \cdot 10^{-17}$	$2.55 \cdot 10^{-17}$	7.01%	8.12%	1.04%

Analysis of fresh soot

The different CAST OP modes show that the mass decreases when the fraction of propane decreases (Figure 11). The mass-mobility exponent (D_m) from equation 3 agrees with Park et al. (2003) although it is slightly lower than the general range of 2.2-2.4, but distinctly far from 3 indicating a non-spherical growth. The lower values can be a result from using a device producing pure particles while the soot analysed by Park et al. (2003) was obtained by real diesel engines where traces of lubricants may be present.

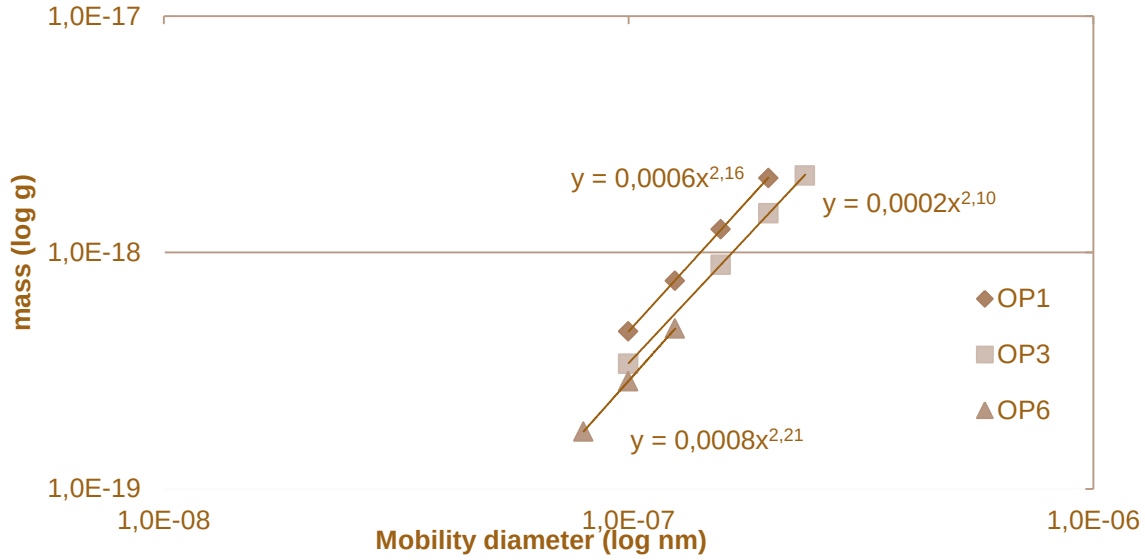

Figure 11 Mass-mobility exponent (D_m) analysis

The mass obtained from the APM is plotted for the selected sizes for each OP mode, both axes are on a logarithmic scale. The exponent of the trend line equations is the D_m variable mentioned in Equation 3 where a value of 3 indicates spherical growth while values less than 3 indicates non-spherical growth.

Alike mass the effective density decreases with increasing OP number (listed in Table 1) and can be seen in Figure 12. Park et al. (2003) used a Transmission Electron Microscope which allowed them to analyse the primary particle structure of their soot. They found that as the size increases, the particles become more irregular and agglomerated. This leads to a decrease in effective density since the mobility diameter in relations to mass grow faster due to the irregular shape, whereas more compact soot with the same number of primary particles would have a higher effective density. The decrease in effective density with increasing OP can be that the lower combustion temperature results in smaller primary particles or more irregular shapes (Park et al., 2003; Moore et al., 2014).

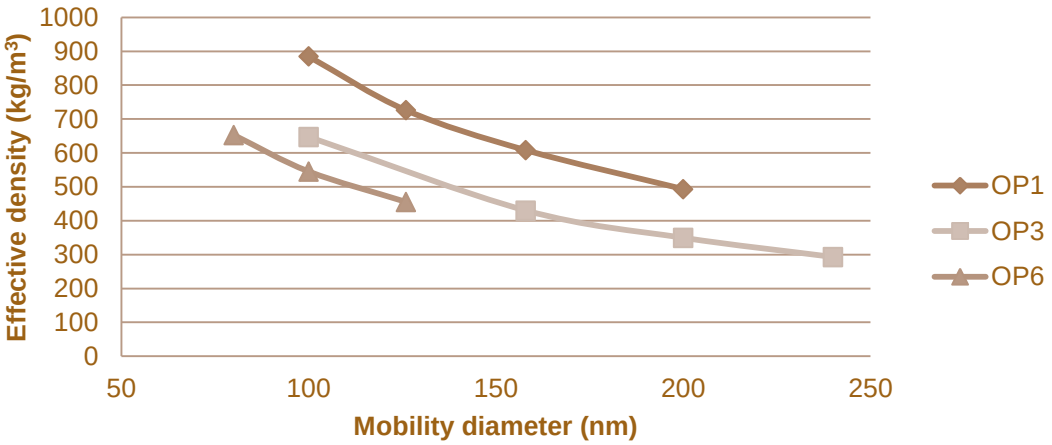

Figure 12 Effective density analysis

The effective density obtained by the relationship in Equation 12 for the mass values in Figure 11 plotted against the size of the particle. The different OP modes are clearly separated and show similar characteristics with decreasing effective density when the particle size increases.

Initial coating stage with single compound

The scans available from the initial coating stage showed an increase of mass by 18% for the initial 126nm soot particle and 24% for the 240nm particle (Figure 13). The greater increase of mass for the larger particle could be explained by the kelvin effect and the larger area of available soot surface.

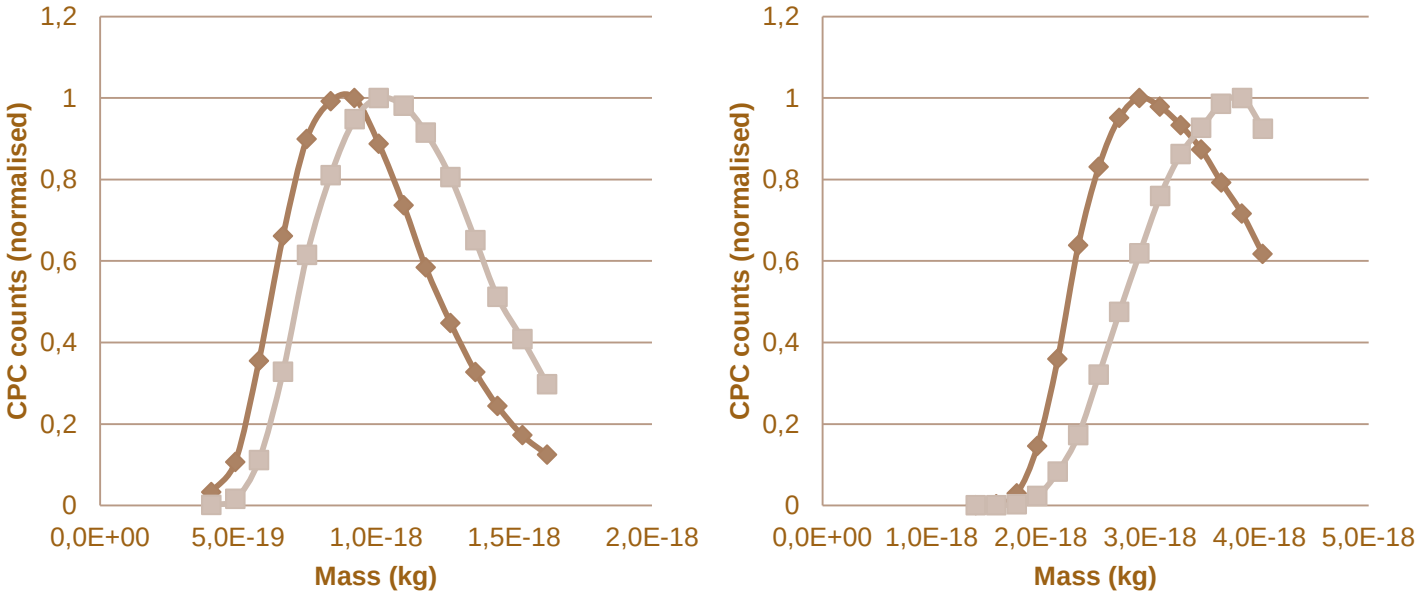

Figure 13 Initial coating experiments

The mass distribution for the two initial Succinic Acid coating experiments, with 126nm to the left and 240nm to the right. The mass distribution for coated soot (squares) grows in mass for both sizes (moves to the right compared to the fresh soot (diamonds)).

These few successful results indicated that the set-up design had potential to fulfil the purpose. However, the set-up was not stable over time which leads to the improvements as described in the method section for coating stage 2.

Improved coating stage with single compounds

Dioctyl Sebacate

The DOS experiments with the improved coating chamber proved positive. The improved soot set-up remained very stable over time where steady state was achieved on a scale of a few minutes after the temperature was changed in the particle generator. The dilution system prevented any clogging in the system and there were no artefacts in the measurements related to residues of leftover soot in any instrument. The temperature was increased with steps of 5-10 °C between 60-120 °C and yielded satisfactory coating levels until nucleation of DOS was achieved at 115C which can be seen in Figure 14. The scan of 120 °C was removed since the CPC was flooded by particles making any soot peak undistinguishable and the 115 °C peak being quite broad and edgy with signs of background counts. The last scan is however still distinctly to the right of the previous coating levels and gives insight even though the coated peak value influenced by what can be a pure DOS peak around $5.0 \cdot 10^{-18}$ kg matching the density of DOS.

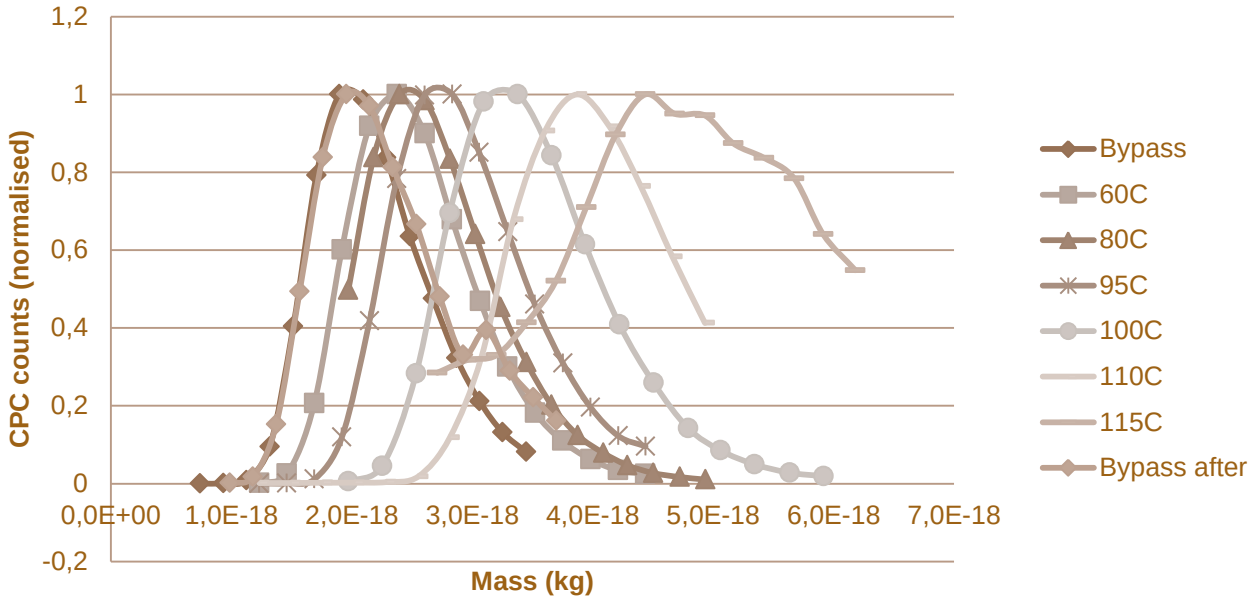

Figure 14 DOS mass analysis
The mass distributions obtained by the APM for the DOS experiments showing that the mass of the particles increase with increasing temperature in the particle generator.

All coating levels before 115 °C show no broadening of the peak meaning that all soot particles are equally coated by DOS whereas Ghazi & Olfert (2013) concluded that they experienced different amount of coating on their particles resulting in a broader distribution. The SMPS scans visualized in Figure 15 presented no distinct changes in mobility diameter even though the mass increased until the last coating level when the size grew from ~201 nm to ~209 nm.

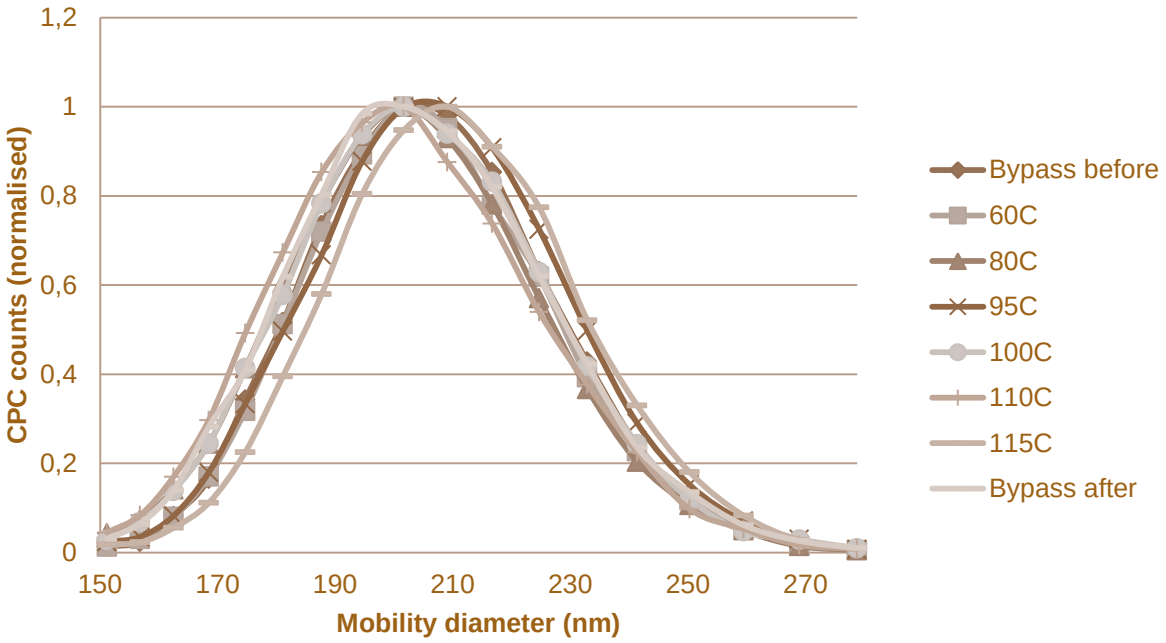

Figure 15 DOS size analysis
The size distribution scanned by the SMPS corresponding to the mass distributions for the temperatures in Figure 14.

The effective density obtained by the mass in Figure 14 and the size in Figure 15 was matched alike Ghazi & Olfert (2013) with a theoretical spherical assumption of a particle growing by the same amount of coating which is illustrated in Figure 16. In their experiments the coated soot reached the spherical assumption at the mass growth factor 6-7 which is far above the levels reached in this experiment.

The resulting effective density of the spherical assumption with the initial soot core (1.77 g/cm^3) and added DOS coating (0.914 g/cm^3) will decrease towards the latter material density when the coating grows to an infinite sphere (where effective density equals material density) since the fraction of soot will be negligible. This is observed in Ghazi & Olfert (2013) and the tendency in this experiment agrees well with theirs. This means that the system used in this experiment agrees well with literature and is valid for further experiments.

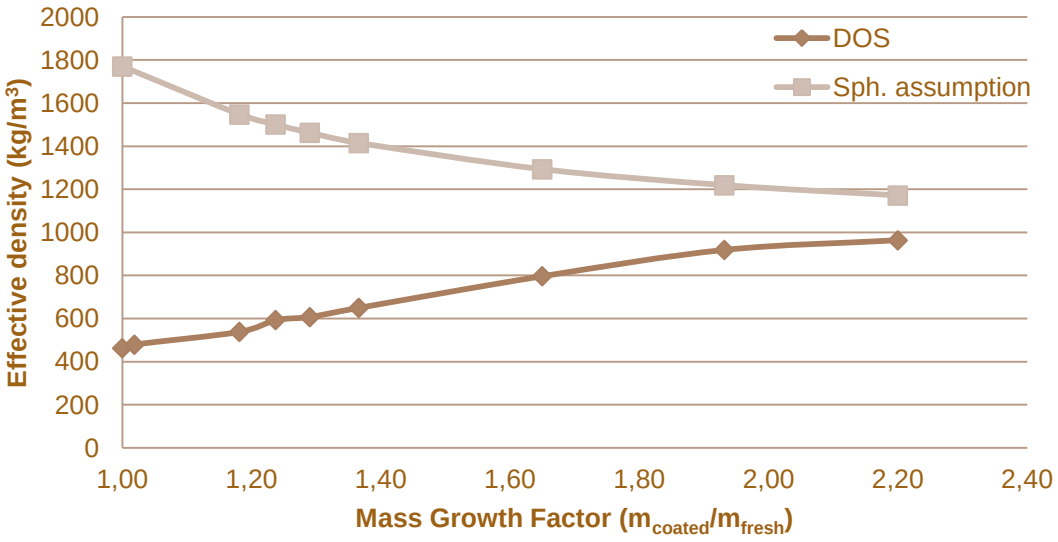

Figure 16 Spherical assumption comparison

The effective density for the DOS experiment plotted with the theoretical spherical assumption of a soot particle of the same size. The measured particle grows towards the spherical assumption as the coating level increases.

Succinic Acid coating

The mass growth for different initial soot sizes coated with Succinic Acid indicates a higher mass growth factor for small particles seen in figure 17.

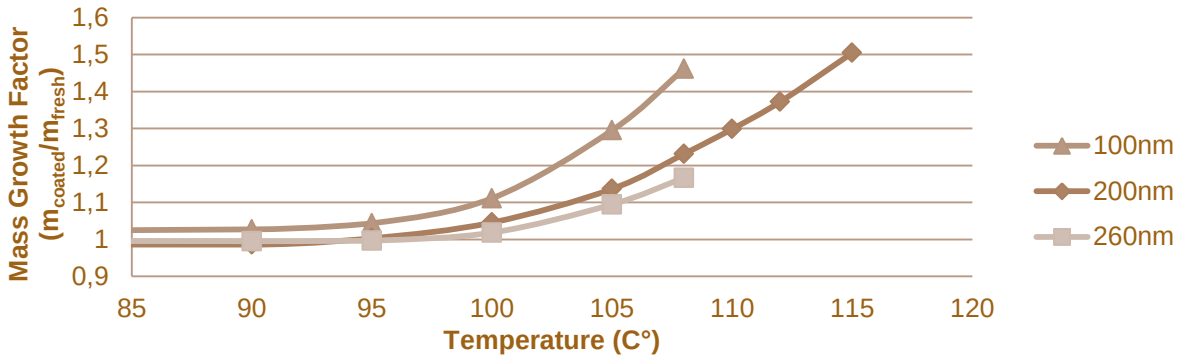

Figure 17 Mass Growth Factor for Succinic Acid coating
The mass growth profiles for the three soot sizes coated with succinic acid. The smallest size, 100nm (triangle) grows the fastest followed by 200nm (diamond) and 260nm (square) being the largest particle growing the slowest.

The change in effective density as seen in Figure 18 does not agree with the theory where the effective density should grow towards the spherical assumption as in the DOS experiment in Figure 16.

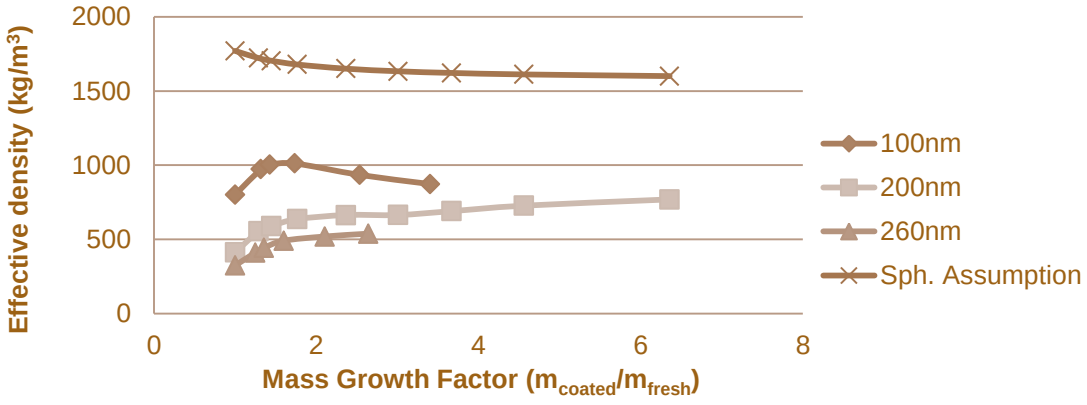

Figure 18 Effective density analysis for Succinic Acid coating
The effective density for soot coated with Succinic Acid plotted against the Mass Growth Factor together with the theoretical spherical assumption of a 200nm soot particle.

The experiments with SA were less successful due to an unexpected high rate of evaporation of succinic acid condensed on the particles in the system affecting the mass analysis. The residence time of the particles is the longest in the APM being around ten seconds compared to the DMA being around one second and negligible in the rest of the system.

The slightly increased temperature in the APM due to the rotating cylinders enhances the evaporation rate which made the mass analysis of SA unreliable. The vapour pressure for liquid succinic acid is presented by Riipinen et al. (2006) as a function of temperature and an increase of ten degrees which may be reached in the APM can cause a big difference in evaporation rate. However the relationship between the sizes can still provide a useful insight to the characteristics of SA and the effects of high relative humidity.

The effect of high relative humidity in the impinger experiment on soot coated with SA is shown in Figure 19 together with the size growth compared to mass growth for the DOS experiment. The curve for SA run through the impinger initially decreases in size while the SA run bypass the impinger show no decrease. At around a 50% growth of mass both curves start a positive trend. This decrease of mobility diameter for the SA run through the impinger is caused by a collapse of the soot core (Pagels et al., 2009).

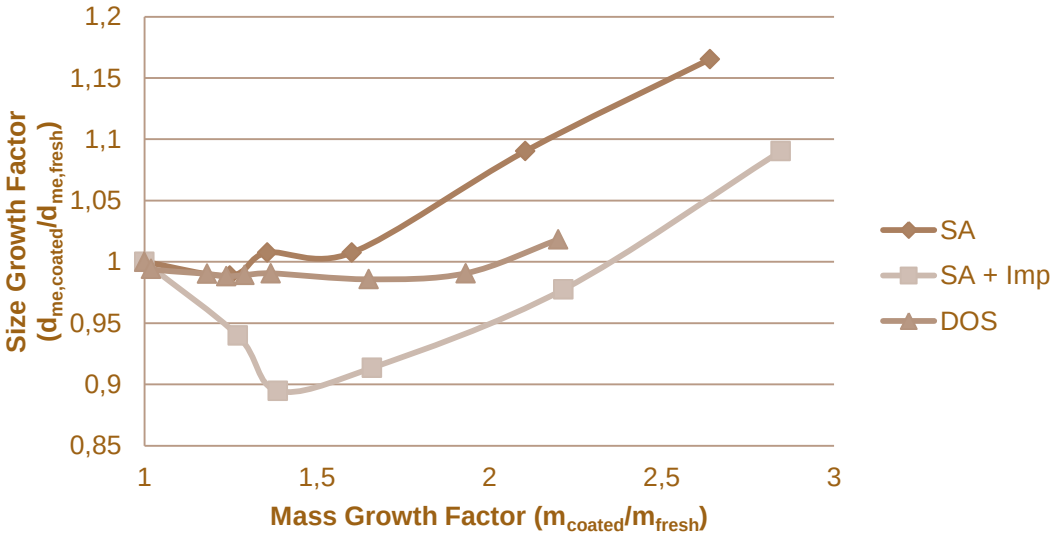

Figure 19 Size Growth Analysis for coating with single compounds

The change in initial mobility diameter with increasing mass growth for Succinic Acid (diamond), Succinic Acid through the Impinger (squre) and DOS (triangle).

The DOS experiment show a tendency in Figure 19 that the coated particles start to decrease in size with a minimum at around 60% mass growth which may

indicate a collapse of the soot core observed by Ghazi & Olfert (2013). They found that the 150nm particles run in their experiment are too small for this collapse to be observed being shadowed by the coating growth. The effects observed in this experiment are however very small.

The coating of the soot cores will affect the absorption capabilities of the particle as discussed by Bond et al. (2006), where the coating will function as a lens focusing the incoming light at the core which could increase the absorption by 100% (Bond et al., 2006; Khalisov et al., 2009; Cross et al., 2010).

Coating with complex Secondary Organic Aerosol using PAM chamber

The final experiment conducted proved very demanding yet with success. Both levels of PAM coating showed an increase of mass, however the SOA generated by alpha-pinene self-nucleated during many trials which were time consuming and time was the limiting factor due to instrumental availability.

In comparison to the DOS coating experiment, the SOA coating generated by the PAM results in a broadening of the mass distributions as seen in Figure 19. This broadening is similar to the one discussed by Ghazi & Olfert (2013) where the coating level is uneven of the particle distribution. Scans were made with the SMPS DMA after the soot dilution system to obtain a monodisperse soot size distribution which proved equally promising as the polydisperse size distribution shown in Figure 20.

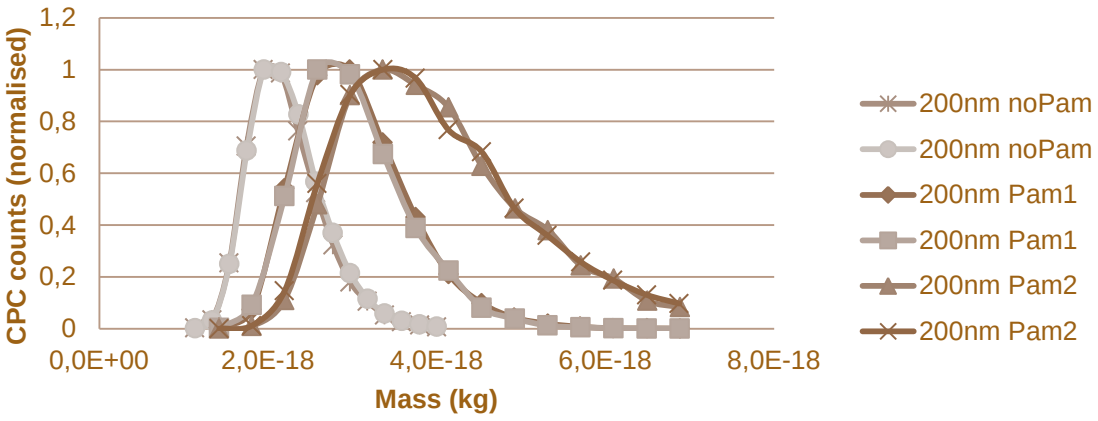

Figure 20 Analysis of PAM SOA coating
The mass distribution for fresh soot (noPam) and two levels of coating with the SOA generated by the alpha-pinene.

The PAM coating experiment was designed in short time and the set-up can be seen as an alpha stage of trials, with this in mind these results indicate the potential of future PAM-APM experiments.

APM Software

The new software for running the APM proved successful by equally matching the old way to run it on an experimental level. The theoretical benefits are greater with a more stable transfer function with the focus on keeping the value of λ_c constant. The main issue with the new software is that the voltage applied in the APM is determined by the program itself and will not let the user set a value for this leading to issues with the RPM boundaries. If the user was allowed to determine this value then scanning small particles with low masses would be possible, at present scanning particles under 80nm is demanding unless the effective density is fairly high.

Another issue is the reaction time between the software and the hardware, the program is set to be very careful not to increase the RPM instantly or too fast and is set to have sufficient amount of time before changing values. These waiting times are far too long (approximately half a minute each) making each individual scan time consuming, optimising these would save time on the scale of minutes per scan for the user.

The idea of varying the rotational speed instead of the voltage was implemented by Olfert and Collings (2005) with the Couette centrifugal Particle Mass Analyser (CPMA). The CPMA is building on similar benefits that Kuwata (2015) proposed but with a technical modification of the APM, the inner rod rotates slightly faster than the outer rod (Olfert & Collings; 2005). The further development of the APM software will be valuable in future experiments.

Conclusion

The new approach of running the APM by varying the RPM proved successful not only in theory but also in practice. The mass measurements offered well defined distributions and showed no indication of conflict between the hardware and software.

Fresh soot was analysed and the effective density was observed to decrease with increasing OP, where increasing OP results in lower combustion temperatures achieved by increasing the flow of cooling gases. The soot mass-mobility exponent was clearly below a value of 3 indicating a non-spherical growth which agrees well with soot characteristics and other experiments (Park et al., 2003; Moore et al., 2014).

The improved set-up for coating soot particles under controlled conditions proved very successful, being very stable over time with distinct coating levels and a steady state achieved after only a few minutes. The set-up was validated by running DOS and similar results were achieved as those by Ghazi & Olfert (2013). The effect of high RH on coated soot was analysed by running the hygroscopic SA through an impinger with mixed results as the SA evaporated in the APM rendering the mass analysis inadequate. The SMPS measurement however recorded a collapse of the soot core coated with SA which is similar to the results found by Pagels et al. (2009).

The PAM experiments displayed potential by successfully coating the soot by SOA generated by alpha-pinene, showing the capability of running the soot set-up with PAM-APM. The set-up is capable of various modifications opening it up for analyses of many compounds and interactions. Further analyses of coated soot can give important information about the absorption rate of light when coated by different substances. The capability of lung deposition when altering the soot structure by collapse and coating can also provide vital knowledge in the future.

The set-up can be used to coat other particles than soot with organic compounds. One such compound of interest could be phthalates which are widely used in building materials and household products. Exposure to phthalates has been linked to health effects such as asthma, allergies and the reproductive development. It is suggested by Benning et al. (2013) that further research is needed to investigate the interaction between phthalates and the chemical composition, size and surface area of airborne particles.

Acknowledgments

First off I would like to thank my supervisor for his never failing mood when it comes to any kind of setbacks, it has been very inspirational to share his compassion for the APM and its possibilities.

Secondly I want extend my gratitude to Axel Eriksson, Erik Ahlberg, Erik Nordin, Jonas Jakobsson and Vilhelm Malmborg for answering all my questions no matter how simple or complex when it comes to instrumental theory. With their support and knowledge I have managed to work independently in the lab with my set-ups and I have felt encouraged to try more variables rather than cutting back which has been a great contribution to my thesis.

Lastly I would like to thank Per-Erik Bengtsson from Combustion Physics at Lund University for letting me use their miniCAST in my experiments.

References

Allen, M. D., and Raabe, O. G. 1982. Re-Evaluation of Millikan Oil Drop Data for the Motion of Small Particles in Air, *J. Aerosol Sci*. 13(6), pp. 537-547.

Allen, M. D., and Raabe, O. G. 1985. Slip Correction Measurements of Spherical Solid Aerosol-Particles in an Improved Millikan Apparatus, *Aerosol Sci. Technol.* 4(3):269-286.

Barone, T. L., Storey, J. M. E., Youngquist, A. D., Szybist, J. P., 2012, An analysis of direct-injection spark-ignition (DISI) soot morphology. *Atmos. Environ.*, 49, pp.268-274.

Benning, J. L., Liu, Z., Tiwari, A., Little, J. C., & Marr, L. C. 2013. Characterizing gas-particle interactions of phthalate plasticizer emitted from vinyl flooring. Environmental science & technology, 47, pp. 2696-2703.

Bond, T. C., Habib, G., & Bergstrom, R. W. 2006. Limitations in the enhancement of visible light absorption due to mixing state. Journal of Geophysical Research: Atmospheres, 111(D20).

Bond, T. C., Doherty, S. J., Fahey, D. W., Forster, P. M., Berntsen, T., DeAngelo, B. J., ... & Kinne, S. 2013. Bounding the role of black carbon in the climate system: A scientific assessment. Journal of Geophysical Research: Atmospheres, 118, pp. 5380-5552.

Cross, E. S., Onasch, T. B.,Ahern, A., Wrobel, W., Slowik, F. G., Olfert, J., Lack, D. A., Massoli, P., Cappa, C. D., Schwarz, J. P., Spackman, J. R., Fahey, D. W., Sedlacek, A., Trimborn, A., Jayne, J. T., Freedman, A., Williams, L. R., Ng, N. L., Mazzoleni, C., Dubey, M., Brem, B., Kok, G., Subramanian, R., Freitag, S., Clarke, A., Thornhill, D., Marr, L. C., Kolb, C. E., Worsnop, D. R., Davidovits, P., 2010, Soot Particle Studies—Instrument Inter-Comparison—Project Overview, *Aerosol Science and Technology*, 44, pp. 592-611

Decarlo, P. F., Slowik, J. G., Worsnop, D. R., Davidovits, P., and Jimenez, J. L. 2004. Particle Morphology and Density Characterization by Combined Mobility and Aerodynamic Diameter Measurements. Part 1: Theory, *Aerosol Sci. Technol*. 38, pp. 1185-1205.

Dekati, 2016a. The Dekati® Diluter DI-1000. [ONLINE] Available at: http://www.dekati.com/products/Aerosol%20Sample%20Conditioning/Dekati%C2%AE%20Diluter [Accessed 21 Mar. 2016].

Dekati, 2016b. The Dekati® Diluter DI-1000. [image] Available at: http://www.dekati.com/products/Aerosol%20Sample%20Conditioning/Dekati%C2%AE%20Diluter [Accessed 21 Mar. 2016].

Ehara, K., Hagwood, C., and Coakley, K. J. 1995. Novel Method to Classify Aerosol Particles According to their Mass-to-Charge Ratio – Aerosol Particle Mass Analyser, *J. Aerosol Sci.* 27, pp. 217-234.

EPA 2012, Report to Congress on Black Carbon, US Environmental Protection Agency, Washington, DC.

Ghazi, R. and Olfert, J. S., 2013, Coating Mass Dependence of Soot Aggregate Restructuring due to Coatings of Oleic Acid and Dioctyl Sebacate, *Aerosol Sci. Technol*. 47, pp. 192-200.

Hinds, W. C. 1999. *Aerosol Technology Properties, Behavior, and Measurement of Airborne Particles*, 2nd ed. Wiley, New York, USA.

JING. 2009. miniCAST Series 5200. [ONLINE] Available at:http://www.sootgenerator.com/midCAST_g.htm. [Accessed 20 March 16].

Kang, E., Root, M. J., Toohey, D. W., Brune, W. H., 2007, Introducing the concept of Potential Aerosol Mass (PAM), *Atmos. Chem. Phys.*, 7, pp. 5727-5744.

Khalizov, A. F., H. X. Xue, L. Wang, J. Zheng, and R. Y. Zhang 2009,

Enhanced light absorption and scattering by carbon soot aerosol internally mixed with sulfuric acid, J. *Phys. Chem. A*, 113, pp. 1066–1074.

Knutson, E. O., and Whitby, K. T. 1975. Aerosol Classification by Electric Mobility: Apparatus, *Theory and Applications. J. Aerosol Sci*., 6, pp. 443–451.

Kuwata, M. 2015. Particle Classification by the Tandem Differential Mobility Analyzer - Particle Mass Analyzer System, *Aerosol Sci. Technol*. 49, pp. 508-520.

Lambe, A. T., Ahern, A. T., Williams, L. R., Slowik, J. G., Wong, J. P. S., Abbatt, J. P. D., Brune, W. H., Ng, N. L., Croasdale, D. R., Wright, J. P., Worsnop, D. R., Dadidovits, P., Onasch, T. B., 2010, Characterization of aerosol photooxidation flow reactors: heterogeneous oxidation, secondary organic aerosol formation and cloud condensation nuclei activity measurements, *Atmos Meas. Tech. Discuss.* 3, pp. 5211-5251.

McMurry, P. H., Wang, X., Park, K., and Ehara, K. 2002. The Relationship between Mass and Mobility for Atmospheric Particles: A New Technique for Measuring Particle Density, *Aerosol Sci. Technol.* 36, pp. 227-238.

Moore, R. H., Ziemba, L. D., Dutcher, D., Beyersdorf, A. J., Chan, K., Crumeyrolle, S., ... & Anderson, B. E. 2014. Mapping the operation of the miniature combustion aerosol standard (Mini-CAST) soot generator. *Aerosol Science and Technology*, *48*, pp. 467-479.

Miljevic, B., Surawski, N. C., Bostrom, T., Ristovski, Z. D. 2011, Restructuring of carbonaceous particles upon exposure to organic and water vapours, *J. Aerosol Sci* 47, pp. 48-57.

Olfert, J. S., and Collings, N. 2005. New Method for Particle Mass Classification – the Couette Centrifugal Particle Mass Analyser, *J. Aerosol Sci.* 36, pp. 1338-1352.

Pagels, J., Khalizov, A. F., McMurry, P. H., and Zhang, R. Y. 2009. Processing of Soot by Controlled Sulphuric Acid and Water Condensation – Mass and Mobility Relationship, *Aerosol Sci. Technol.* 43, pp. 629-640.

Park, K., Cao, F., Kittelson, D. B., and McMurry, P. H. 2003. Relationship Between Particle Mass and Mobility for Diesel Exhaust Particles, *Environ. Sci. Technol*. 37, pp. 577-583.

Park, K., Kittelson, D. B., and McMurry, P. H. 2004a. Structural Properties of Diesel Exhaust Particles Measured by Transmission Electron Microscopy (TEM): Relationships to Particle Mass and Mobility, *Aerosol Sci. Technol.* 38, pp. 881-889.

Park, K., Kittelson, D. B., Zachariah, M. R., and McMurry, P. H. 2004b. Measurement of Inherent Material Density of Nanoparticle Agglomerates, *J. Nanopart. Res.* 6, pp. 267-272.

Pubchem. 2016. BIS(2-ETHYLHEXYL) SEBACATE. [ONLINE] Available at:https://pubchem.ncbi.nlm.nih.gov/compound/31218. [Accessed 20 March 16].

Pubchem. 2016. Succinic Acid. [ONLINE] Available at:https://pubchem.ncbi.nlm.nih.gov/compound/succinic_acid. [Accessed 20 March 16].

Schnitzler, E. G., Dutt, A., Charbonneau, A. M., Olfert, J. S., & Jäger, W. 2014. Soot aggregate restructuring due to coatings of secondary organic aerosol derived from aromatic precursors. *Environmental science & technology*, *48*(24), pp. 14309-14316.

Tajima, N., Fukushima, N., Ehara, K., and Sakurai, H. 2011. Mass Range and Optimized Operation of the Aerosol Particle Mass Analyzer, Aerosol Sci. Technol. 45, pp. 196-214.

TOPAS. 2016. SLG 250, 270 - Monodisperse Aerosol Generator. [ONLINE] Available at:http://www.topas-gmbh.de/en/produkte/slg-250/. [Accessed 20 March 16].

Totton, T. S., Chakrabarti, D., Misquitta, A. J., Sander, M., Wales, D. J., Kraft, M. 2010. Modelling the internal structure of nascent soot particles. *Combust. Flame* 157, pp. 909-914

Zhang, R., Khalizov, A. F., Pagels, J., Zhang, D., Xue, Huaxin., and McMurry, P. H. 2008. Variability in morphology, hygroscopicity, and optical properties of soot aerosols during atmospheric processing, *Proc. Natl. Acad. Sci. U. S. A.*, 105, pp. 10291–10296.

Appendix I

APM

			Vektor	Particle size																	
s	m (Kg)	e (C)	råeff (Kg/	dme (m)	Pi	rc (m)	r1 (m)	r2 (m)	tao	L (m)	v-mean a	my (Pa/s)	Q (m3/s)	Area yttre	Area inre	B	Cc	l (mean fr	Kn	2pi/30	n of charg
3,444901	5,52E-19	1,6E-19	1054	0,0000001	3,141593	0,051	0,05	0,052	8,5E-08	0,25	0,055663	2E-05	1,8E-05	0,004247	0,003927	1,54E+11	2,878049	6,73E-08	1,346	0,10472	1
3,444901	5,52E-19	1,6E-19	1054	0,0000001	3,141593	0,051	0,05	0,052	8,5E-08	0,25	0,055663	2E-05	1,8E-05	0,004247	0,003927	1,54E+11	2,878049	6,73E-08	1,346	0,10472	1
3,444901	5,52E-19	1,6E-19	1054	0,0000001	3,141593	0,051	0,05	0,052	8,5E-08	0,25	0,055663	2E-05	1,8E-05	0,004247	0,003927	1,54E+11	2,878049	6,73E-08	1,346	0,10472	1
3,444901	5,52E-19	1,6E-19	1054	0,0000001	3,141593	0,051	0,05	0,052	8,5E-08	0,25	0,055663	2E-05	1,8E-05	0,004247	0,003927	1,54E+11	2,878049	6,73E-08	1,346	0,10472	1
3,444901	5,52E-19	1,6E-19	1054	0,0000001	3,141593	0,051	0,05	0,052	8,5E-08	0,25	0,055663	2E-05	1,8E-05	0,004247	0,003927	1,54E+11	2,878049	6,73E-08	1,346	0,10472	1
3,444901	5,52E-19	1,6E-19	1054	0,0000001	3,141593	0,051	0,05	0,052	8,5E-08	0,25	0,055663	2E-05	1,8E-05	0,004247	0,003927	1,54E+11	2,878049	6,73E-08	1,346	0,10472	1
3,444901	5,52E-19	1,6E-19	1054	0,0000001	3,141593	0,051	0,05	0,052	8,5E-08	0,25	0,055663	2E-05	1,8E-05	0,004247	0,003927	1,54E+11	2,878049	6,73E-08	1,346	0,10472	1
3,444901	5,52E-19	1,6E-19	1054	0,0000001	3,141593	0,051	0,05	0,052	8,5E-08	0,25	0,055663	2E-05	1,8E-05	0,004247	0,003927	1,54E+11	2,878049	6,73E-08	1,346	0,10472	1
3,444901	5,52E-19	1,6E-19	1054	0,0000001	3,141593	0,051	0,05	0,052	8,5E-08	0,25	0,055663	2E-05	1,8E-05	0,004247	0,003927	1,54E+11	2,878049	6,73E-08	1,346	0,10472	1
3,444901	5,52E-19	1,6E-19	1054	0,0000001	3,141593	0,051	0,05	0,052	8,5E-08	0,25	0,055663	2E-05	1,8E-05	0,004247	0,003927	1,54E+11	2,878049	6,73E-08	1,346	0,10472	1
3,444901	5,52E-19	1,6E-19	1054	0,0000001	3,141593	0,051	0,05	0,052	8,5E-08	0,25	0,055663	2E-05	1,8E-05	0,004247	0,003927	1,54E+11	2,878049	6,73E-08	1,346	0,10472	1
3,444901	5,52E-19	1,6E-19	1054	0,0000001	3,141593	0,051	0,05	0,052	8,5E-08	0,25	0,055663	2E-05	1,8E-05	0,004247	0,003927	1,54E+11	2,878049	6,73E-08	1,346	0,10472	1
3,444901	5,52E-19	1,6E-19	1054	0,0000001	3,141593	0,051	0,05	0,052	8,5E-08	0,25	0,055663	2E-05	1,8E-05	0,004247	0,003927	1,54E+11	2,878049	6,73E-08	1,346	0,10472	1
3,444901	5,52E-19	1,6E-19	1054	0,0000001	3,141593	0,051	0,05	0,052	8,5E-08	0,25	0,055663	2E-05	1,8E-05	0,004247	0,003927	1,54E+11	2,878049	6,73E-08	1,346	0,10472	1
3,444901	5,52E-19	1,6E-19	1054	0,0000001	3,141593	0,051	0,05	0,052	8,5E-08	0,25	0,055663	2E-05	1,8E-05	0,004247	0,003927	1,54E+11	2,878049	6,73E-08	1,346	0,10472	1

Test Lambda			
Lambda	Omega	OmegaRP	V
0,1	361,9327	3456,203	46,03501
0,2	511,8502	4887,809	92,07003
0,3	626,8859	5986,319	138,105
0,4	723,8655	6912,406	184,1401
0,5	809,3062	7728,305	230,1751
0,6	886,5505	8465,934	276,2101
0,7	957,584	9144,254	322,2451
0,8	1023,7	9775,618	368,2801
0,9	1085,798	10368,61	414,3151
1	1144,532	10929,47	460,3501
1,1	1200,395	11462,93	506,3852
1,2	1253,772	11972,64	552,4202
1,3	1304,967	12461,52	598,4552
1,4	1354,228	12931,93	644,4902
1,5	1401,759	13385,82	690,5252

DMA

Sheath flow											DMA Voltage		
Q (m3/s)	r2 (m)	r1 (m)	L (m)	Pi	Cc	l (mean fr	Kn	my (Pa/s)	e (C)	Z*	V	dme (m)	n of charg
0,0001	0,01958	0,00937	0,4444	3,14159265	2,878049	6,73E-08	1,346	2E-05	1,6E-19	2,47E-08	1070,116	1E-07	1
0,0001	0,01958	0,00937	0,4444	3,14159265	2,878049	6,73E-08	1,346	2E-05	1,6E-19	2,47E-08	1070,116	1E-07	1
0,0001	0,01958	0,00937	0,4444	3,14159265	2,878049	6,73E-08	1,346	2E-05	1,6E-19	2,47E-08	1070,116	1E-07	1
0,0001	0,01958	0,00937	0,4444	3,14159265	2,878049	6,73E-08	1,346	2E-05	1,6E-19	2,47E-08	1070,116	1E-07	1
0,0001	0,01958	0,00937	0,4444	3,14159265	2,878049	6,73E-08	1,346	2E-05	1,6E-19	2,47E-08	1070,116	1E-07	1
0,0001	0,01958	0,00937	0,4444	3,14159265	2,878049	6,73E-08	1,346	2E-05	1,6E-19	2,47E-08	1070,116	1E-07	1
0,0001	0,01958	0,00937	0,4444	3,14159265	2,878049	6,73E-08	1,346	2E-05	1,6E-19	2,47E-08	1070,116	1E-07	1
0,0001	0,01958	0,00937	0,4444	3,14159265	2,878049	6,73E-08	1,346	2E-05	1,6E-19	2,47E-08	1070,116	1E-07	1
0,0001	0,01958	0,00937	0,4444	3,14159265	2,878049	6,73E-08	1,346	2E-05	1,6E-19	2,47E-08	1070,116	1E-07	1
0,0001	0,01958	0,00937	0,4444	3,14159265	2,878049	6,73E-08	1,346	2E-05	1,6E-19	2,47E-08	1070,116	1E-07	1
0,0001	0,01958	0,00937	0,4444	3,14159265	2,878049	6,73E-08	1,346	2E-05	1,6E-19	2,47E-08	1070,116	1E-07	1
0,0001	0,01958	0,00937	0,4444	3,14159265	2,878049	6,73E-08	1,346	2E-05	1,6E-19	2,47E-08	1070,116	1E-07	1
0,0001	0,01958	0,00937	0,4444	3,14159265	2,878049	6,73E-08	1,346	2E-05	1,6E-19	2,47E-08	1070,116	1E-07	1
0,0001	0,01958	0,00937	0,4444	3,14159265	2,878049	6,73E-08	1,346	2E-05	1,6E-19	2,47E-08	1070,116	1E-07	1
0,0001	0,01958	0,00937	0,4444	3,14159265	2,878049	6,73E-08	1,346	2E-05	1,6E-19	2,47E-08	1070,116	1E-07	1

Omega-vektor				
Mass (Kg)	V - approp	Omega (ra	OmegaRP	Lambda
3,61E-17	230,1751	100	954,9297	0,5
1,61E-17	230,1751	150	1432,394	0,5
9,04E-18	230,1751	200	1909,859	0,5
5,78E-18	230,1751	250	2387,324	0,5
4,02E-18	230,1751	300	2864,789	0,5
2,95E-18	230,1751	350	3342,254	0,5
2,26E-18	230,1751	400	3819,719	0,5
1,79E-18	230,1751	450	4297,183	0,5
1,45E-18	230,1751	500	4774,648	0,5
1,19E-18	230,1751	550	5252,113	0,5
1E-18	230,1751	600	5729,578	0,5
8,56E-19	230,1751	650	6207,043	0,5
7,38E-19	230,1751	700	6684,508	0,5
6,43E-19	230,1751	750	7161,972	0,5
5,65E-19	230,1751	800	7639,437	0,5

V-vektor				
Mass	V	Omega	OmegaRP	Lambda
1,62E-19	55	730	6970,987	0,119474
1,77E-19	60	730	6970,987	0,130336
1,92E-19	65	730	6970,987	0,141197
2,06E-19	70	730	6970,987	0,152058
2,21E-19	75	730	6970,987	0,162919
2,36E-19	80	730	6970,987	0,173781
2,5E-19	85	730	6970,987	0,184642
2,65E-19	90	730	6970,987	0,195503
2,8E-19	95	730	6970,987	0,206365
2,95E-19	100	730	6970,987	0,217226
3,09E-19	105	730	6970,987	0,228087
3,24E-19	110	730	6970,987	0,238949
3,39E-19	115	730	6970,987	0,24981
3,54E-19	120	730	6970,987	0,260671
3,68E-19	125	730	6970,987	0,271532

Figure I1 Calculation sheet for equation 1 and 4-11

The parameters and values used in equation 1 and 4-11 to obtain reference values for arbitrary characteristics between: masses, mobility diameters and effective densities.

Appendix II

The PSL calibration indicated that the DMA-CPC output which can be seen in Table II1 well agreed with the theoretical assumption for the smaller sizes. For larger particles the voltage offset was between 6-8%.

Table II1 DMA voltage offset

The voltage offset compared to the theoretical value.

PSL Size	Theoretical voltage	Measured voltage	Offset (Measured/Theroretical)
80nm	723.7	737.3	1.9%
100nm	1070	1071.6	0.15%
240nm	4350	4015.6	-7.7%
350nm	7373	6912.5	-6.2%

Appendix III

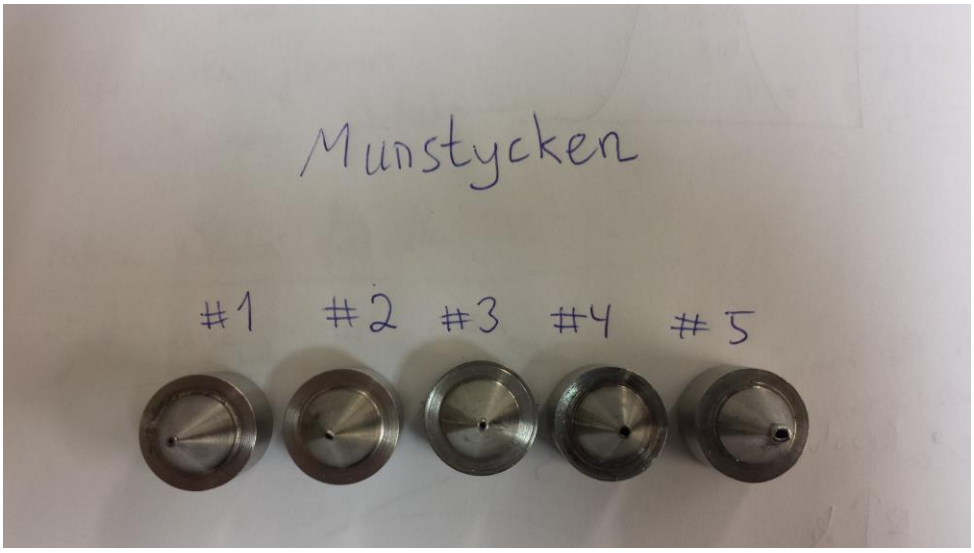

Figure III1 Nozzle classification

The nozzles (SWE=Munstycken) and their number given in order by flow rate.

The nozzle selection available for the experiments is seen in Figure III1 and the measured flow rates which is proportional to the dilution efficiency for each nozzle is noted in Table III1.

Table III1 Nozzle analysis

The measured flow rates and the ratio for each nozzle for 1 bar, 1.5 bar and 2 bar.

Pressure		**1bar**			**1.5bar**			**2bar**	
Nozzle	Before (lpm)	After (lpm)	Ratio	Before (lpm)	After (lpm)	Ratio	Before (lpm)	After (lpm)	Ratio
1	0.580	26.0	44.8	0.63	33.7	53.4	0.65	40.3	62.0
2	1.83	27.9	15.2	2.20	35.5	16.1	2.55	42.2	16.5
3	1.87	27.6	14.8	2.42	35.6	14.7	2.93	42.4	14.5
4	7.97	33.2	4.16	9.92	42.4	4.27	11.7	50.8	4.36
5	11.3	2.45	0.22	16.1	2.65	0.164	20.5	3.05	0.149